J|A|C|S
ARTICLES
Published on Web 01/25/2007

Array of Molecularly Mediated Thin Film Assemblies of Nanoparticles: Correlation of Vapor Sensing with Interparticle Spatial Properties

Lingyan Wang,[†] Xiajing Shi,[‡] Nancy N. Kariuki,[†] Mark Schadt,[†] Guannan Roger Wang,[†] Qiang Rendeng,[†] Jeongku Choi,[†] Jin Luo,[†] Susan Lu,[‡] and Chuan-Jian Zhong*[,†]

Contribution from the Department of Chemistry and Department of System and Industrial Engineering, State University of New York at Binghamton, Binghamton, New York 13902

Received October 11, 2006; E-mail: cjzhong@binghamton.edu

Abstract: The ability to tune interparticle spatial properties of nanoparticle assemblies is essential for the design of sensing materials toward desired sensitivity and selectivity. This paper reports findings of an investigation of molecularly mediated thin film assemblies of metal nanoparticles with controllable interparticle spatial properties as a sensing array. The interparticle spatial properties are controlled by a combination of α,ω-difunctional alkyl mediators ($X-(CH_2)_n-X$) such as alkyl dithiols, dicarboxylate acids, and alkanethiol shells capped on nanoparticles. Alkanethiolate-capped gold and gold−silver alloy nanoparticles (2−3 nm) were studied as model building blocks toward the thin film assemblies, whereas the variation of alkyl chain length manipulates the interparticle spacing. The thin films assembled on an interdigitated microelectrode array platform are characterized for determining their responses to the sorption of volatile organic compounds (VOCs). The correlation between the response sensitivity and the interparticle spacing properties revealed not only a clear dependence of the sensitivity on alkyl chain length but also the occurrence of a dramatic change of the sensitivity in a region of chain length for the alkyl mediator comparable with that of the capping alkyl chains. This finding reflects a balance between the interparticle chain−chain cohesive interdigitation and the nanostructure−vapor interaction which determines the relative change of the electrical conductivity of the inked nanoparticle thin film in response to vapor sorption. The results, along with statistical analysis of the sensor array data in terms of sensitivity and selectivity, have provided important insights into the detailed delineation between the interparticle spacing and the nanostructured sensing properties.

The interparticle physical or chemical properties of molecularly capped nanoparticles have been explored for chemical or biological sensing in a number of significant ways.[1−11] Since the first report on spraying alkanethiolate-protected nanoparticles as a metal−insulator−metal ensemble on chemiresistors for vapor sensing,[2] a number of nanoparticle-structured thin films, including our own work, have been demonstrated to be viable for chemical sensing.[3−11] One example is the use of carboxylate−Cu^{2+}−carboxylate bridged nanoparticles via a swelling-induced alteration in chemical nature to tune electron tunneling.[8] Another example is a molecularly mediated thin film assembly of nanoparticles via covalent bonding or hydrogen bonding of mediator (or linking) molecules on chemiresistive or piezoelectric sensing platforms.[6] Such interparticle-linked thin film nanostructures were recently shown to be viable for constructing a sensing array when the array is coupled to a pattern recognition engine.[12,13] Core−shell type nanoparticles, which are broadly defined as a nanocrystal core and molecular shell of different matters in close interaction[14] or narrowly defined as metal nanocrystal cores capped by an alkanethiolate monolayer shell

[†] Department of Chemistry.
[‡] Department of System and Industrial Engineering.

(1) (a) Templeton, A. C.; Wuelfing, W. P.; Murray, R. W. *Acc. Chem. Res.* **2000**, *33*, 27. (b) Daniel, M.-C.; Astruc, D. *Chem. Rev.* **2004**, *104*, 293. (c) Zhong, C. J.; Han, L.; Kariuki, N. N.; Maye, M. M.; Luo, J. In *Nanoparticle Assemblies and Superstructure*; Kotov, N., Ed.; Marcel Decker Publishers: 2005.
(2) Wohltjen, H.; Snow, A. W. *Anal. Chem.* **1998**, *70*, 2856.
(3) Evans, S. D.; Johnson, S. R.; Cheng, Y. L.; Shen, T. *J. Mater. Chem.* **2000**, *10*, 183.
(4) Severin, E. J.; Lewis, N. S. *Anal. Chem.* **2000**, *72*, 2008.
(5) Shinar, R.; Liu, G. J.; Porter, M. D. *Anal. Chem.* **2000**, *72*, 5981.
(6) Han, L.; Daniel, D. R.; Maye, M. M.; Zhong, C. J. *Anal. Chem.* **2001**, *73*, 4441.
(7) Houser, E. J.; Mlsna, T. E.; Nguyen, V. K.; Chung, R.; Mowery, R. L.; McGill, R. A. *Talanta* **2001**, *54*, 469.
(8) (a) Zamborini, F. P.; Leopold, M. C.; Hicks, J. F.; Kulesza, P. J.; Malik, M. A.; Murray, R. W. *J. Am. Chem. Soc.* **2002**, *124*, 8958. (b) Zamborini, F. P.; Smart, L. E.; Leopold, M. C.; Murray, R. W. *Anal. Chim. Acta* **2003**, *496*, 3.
(9) Cai, Q. Y.; Zellers, E. T. *Anal. Chem.* **2002**, *74*, 3533.
(10) Grate, J. W.; Nelson, D. A.; Skaggs, R. *Anal. Chem.* **2003**, *75*, 1868.
(11) (a) Joseph, Y.; Besnard, I.; Rosenberger, M.; Guse, B.; Nothofer, H.-G.; Wessels, J. M.; Wild, U.; Knop-Gericke, A.; Su, D.; Schloegl, R.; Yasuda, A.; Vossmeyer, T. *J. Phys. Chem. B* **2003**, *107*, 7406. (b) Joseph, Y.; Krasteva, N.; Besnard, I.; Guse, B.; Rosenberger, M.; Wild, U.; Knop-Gericke, A.; Schlogl, R.; Krustev, R.; Yasuda, A.; Vossmeyer, T. *Faraday Discuss.* **2004**, *125*, 77. (c) Joseph, Y.; Guse, B.; Yasuda, A.; Vossmeyer, T. *Sens. Actuators B* **2004**, *98*, 188.
(12) (a) Han, L.; Shi, X.; Wu, W.; Kirk, F. L.; Luo, J.; Wang, L.Y.; Mott, D.; Cousineau, L.; Lim, S. I.-I.; Lu, S.; Zhong, C. J. *Sens. Actuators B* **2005**, *106*, 431. (b) Shi, X.; Wang, L. Y.; Kariuki, N. N.; Luo, J.; Zhong, C. J.; Lu, S. *Sens. Actuators B* **2006**, *117*, 65.
(13) Wang, L. Y.; Kariuki, N. N.; Schadt, M.; Mott, D.; Luo, J.; Zhong, C. J.; Shi, X.; Zhang, C.; Hao, W. B.; Lu, S.; Kim, N.; Wang, J. *Sensors* **2006**, *6*, 667.
(14) Zhong, C. J.; Maye, M. M. *Adv. Mater.* **2001**, *13*, 1507.

Scheme 1. Illustrations of a Chemiresistor Coated with Thin Film Assemblies of Au and AuAg Nanoparticles Mediated by $HS-(CH_2)_n-SH$ and $HOOC-(CH_2)_n-COOH$ of Different Chain Lengths in a Sensor Array

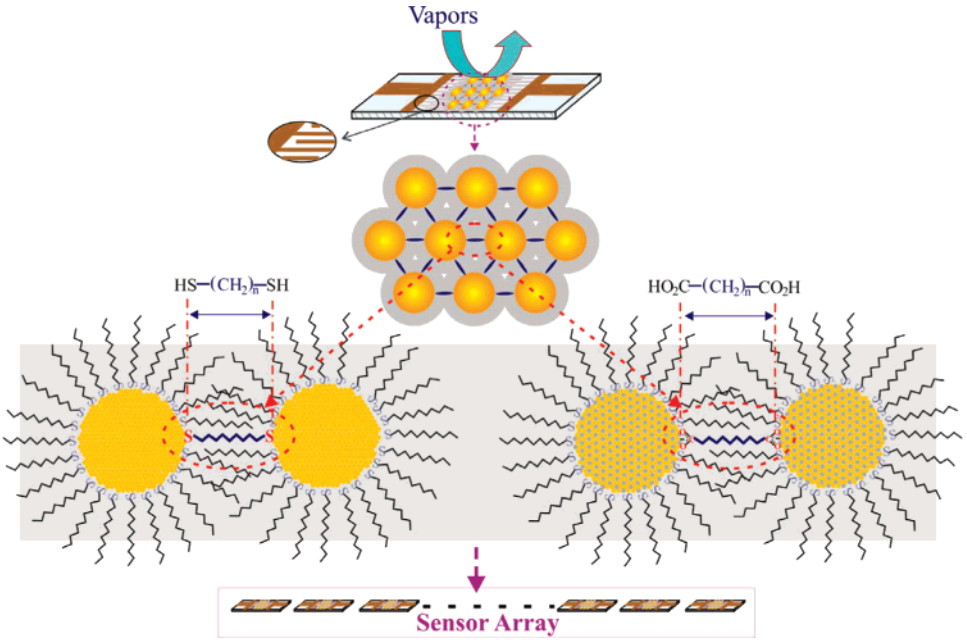

in this work, are intriguing building blocks to sensing array materials because the ability to tune size, composition, functional group, and interparticle spatial properties provides effective ways to enhance sensitivity, selectivity, detection limit, and response time.[15−22] Such an enhancement stems from several important attributes of the nanoparticle assemblies, including the enrichment of ligands or voids in the high surface area-to-volume ratio nanoporous framework for signal amplifications, and the tunability of weak chemical interactions within the molecular linking/capping structures such as hydrogen bonding, ligand coordination, and van der Waals attractive forces. Some elements of these attributes have been demonstrated in our earlier work on nanostructured ion-gating channels with biomimetic specificity,[23] which parallels synthetic or biological receptors.[24] The coupling of these attributes to the semiconductive character of the inked nanoparticle thin film assembly provides a novel pathway to design sensing array materials, which can be implemented with a chemiresistive platform with easy array integration and low power-driven capability.

A key element for using nanostructured thin film materials to design chemiresistive sensing arrays is the correlation between the electrical conductivity and the nanostructural parameters including particle core radius, interparticle distance, and dielectric constant of the interparticle medium. These parameters determine the activation energy in a thermally activated conduction path[25,26] and, thus, have an important impact on the electrical signal amplification in sensing applications. To our knowledge, little has been reported on such a correlation. Built upon our recent successful demonstration of molecularly mediated thin film assemblies of monometallic gold (Au) and bimetallic gold−silver (AuAg) nanoparticles with alkyl dithiols and dicarboxylic acids of different chain lengths,[27] we demonstrate herein the use of these two types of spatially controlled thin film nanostructures as sensing array materials toward establishing the correlation between the chemiresistive responses to the sorption of volatile organic compounds (VOCs) and the interparticle spatial properties. In these nanostructures, Au or AuAg nanoparticles capped with alkanethiolate monolayer shells serve as the building blocks, whereas the alkyl dithiols or dicarboxylic acids of different chain lengths define the interparticle spacing in the molecularly mediated thin film assembly. It is important to emphasize that the capability of thin film assembly by interparticle linking with mediator molecules of different lengths distinguishes our approach from other existing approaches based on casting or spraying to constructing the sensing materials (i.e., unlinked nanoparticles). For the thin film assembly of Au nanoparticles mediated by an alkyl dithiol (ADT, $HS-(CH_2)_n-SH$), the interparticle linkage is formed by Au−thiolate bonds at both ends of the dithiol. For the thin film assembly of AuAg nanoparticles mediated by a dicarboxylic acid (DCA, $HOOC-(CH_2)_n-COOH$), the interparticle linkage is formed by selective ionic binding between carboxylates of the linker and the Ag sites of the bimetallic nanoparticles. These thin film assemblies derived from interparticle linking by the alkyl mediators of different chain lengths form the basis for the design of the sensing array nanomaterials in terms of the interparticle spatial properties (Scheme 1).

While the thin film assemblies of gold and gold−silver alloy nanoparticles using ADTs and DCAs with different alkyl chain

(15) Krasteva, N.; Guse, B.; Besnard, I.; Yasuda, A.; Vossmeyer, T. *Sens. Actuators B* **2003**, *92*, 137.
(16) Leopold, M. C.; Donkers, R. L.; Georganopoulou, D.; Fisher, M.; Zamborini, F. P.; Murray, R. W. *Faraday Discuss.* **2004**, *125*, 63.
(17) Ahn, H. J.; Chandekar, A.; Kang, B. W.; Sung, C. M.; Whitten, J. E. *J. Macromol. Sci., Pure Appl. Chem.* **2005**, *A42*, 1477.
(18) Lavine, B.; Workman, J. *Anal. Chem.* **2006**, *78*, 4137.
(19) Yang, C. Y.; Li, C. L.; Lu, C. J. *Anal. Chim. Acta* **2006**, *565*, 17.
(20) Ibanez, F. J.; Gowrishetty, U.; Crain, M. M.; Walsh, K. M.; Zamborini, F. P. *Anal. Chem.* **2006**, *78*, 753.
(21) Pang, P. F.; Guo, J. L.; Wu, S. H.; Cai, Q. Y. *Sens. Actuators B* **2006**, *114*, 799.
(22) Franke, M. E.; Koplin, T. J.; Simon, U. *Small* **2006**, *2*, 36.
(23) Zheng, W. X.; Maye, M. M.; Leibowitz, F. L.; Zhong, C. J. *Anal. Chem.* **2000**, *72*, 2190.
(24) Dickert, F. L.; Keppler, M.; Zwissler, G. K.; Obermeier, E. *Ber. Bunsen-Ges. Phys. Chem.* **1996**, *100*, 1312.
(25) Hostetler, M. J.; Templeton, A. C.; Murray, R. W. *Langmuir.* **1999**, *15*, 3782.
(26) Abeles, B.; Cheng, P.; Coutts, M. D.; Arie, Y. *Adv. Phys.* **1975**, *24*, 407.

lengths (n, i.e., number of methylenes in the alkyl chain) are different in terms of the binding nature and the building block composition, the similarly tunable alkyl chain length is the common character which provides an important means for the correlation between the sensing array responses to VOCs and the interparticle spatial parameters. The evaluation of the thin films assembled on an interdigitated microelectrode (IME) array for the detection of VOCs and the coupling of the array data processing with pattern recognition techniques such as Principal Component Analysis (PCA) and Artificial Neural Networks (ANN)[28] should provide important insights into the detailed delineation of the interparticle spatial design parameters for constructing nanostructured sensing arrays.

Experimental Section

Chemicals. Hydrogen tetrachloroaurate trihydrate ($HAuCl_4 \cdot 3H_2O$, 99%), silver nitrate ($AgNO_3$, 99+%), potassium bromide (KBr, 99+%), tetraoctylammonium bromide (TOA^+Br^-, 99%), decanethiol (DT, 96%), and sodium borohydride ($NaBH_4$, 99%) were purchased from Aldrich. Alkyl dithiols (ADT, $HS-(CH_2)_n-SH$), such as 1,3-propanedithiol ($n = 3$, 99%), 1,5-pentanedithiol ($n = 5$, 96%), 1,8-octanedithiol ($n = 8$, 97%), and 1,9-nonadithiol ($n = 9$, 95%), were purchased from Aldrich and used as received. 1,10-Decanedithiol ($n = 10$, 90%) was purchased from TCI and used as received. Dicarboxylic acids (DCA, $HO_2C-(CH_2)_n-CO_2H$) such as dodecanedioic acid ($n = 10$, 99%) and 1,14-tetradecanedicarboxylic acid ($n = 14$, 96%) were purchased from Aldrich. 1,12-Dodecanedicarboxylic acid ($n = 12$, 98%), 1,13-tridecanedicarboxylic acid ($n = 13$, 97%), 1,16-hexadecanedicarboxylic acid ($n = 16$, 97%), and 1,18-octadecanedicarboxylic acid ($n = 18$, 99%) were purchased from TCI and used as received. Solvents such as hexane (99.9%) and toluene (99.8%) were purchased from Fisher, and ethanol (99.9%) was purchased from Aldrich. Water was purified with a Millipore Milli-Q water system. The tested organic vapors were generated from solvents of hexane (Hx, 99.9%, Fisher), benzene (Bz, 99.0%, Fisher, carcinogenic), and toluene (Tl, 99.9%, J. T. Baker).

Synthesis of Nanoparticles. Au nanoparticles of 2 nm core size encapsulated with decanethiolate (DT) monolayer shell were synthesized by two-phase reduction of $AuCl_4^-$ according to Brust's method[30a] and a synthetic modification.[30b] Details for the synthesis of our gold nanoparticles (2.0 ± 0.7 nm core size) were previously described.[30c] AuAg alloy nanoparticles capped with a DT monolayer shell were synthesized by two-phase reduction of $AuCl_4^-$ and $AgBr_2^-$ according to a method developed recently in our laboratory. Details for the synthesis of AuAg nanoparticles of various bimetallic composition (0−100% Ag) and (2.0−3.0) ± 0.5 nm core sizes were recently reported.[31] AuAg nanoparticles with a Au/Ag ratio of 1:3 in the nanoparticle were used in this work.

Preparation of Thin Film Assembly. The general preparation of the thin films followed the one-step exchange-crosslinking-precipitation method reported for gold[6,27b] and AuAg nanoparticles.[27c] Briefly, it involved immersion of substrates (e.g., glass, electrodes, etc.) into a hexane solution of DT-capped Au (30 μM) and ADT (50 mM) for the ADT-mediated assembly of Au nanoparticles (i.e., ADT−Au film), or a mixture of a hexane solution of DT-capped AuAg nanoparticles (1.0 μM) and ethanol or tetrahydrofuran solution of DCA (20 mM) for the DCA-mediated assembly of AuAg nanoparticles (i.e., DCA−AuAg film). The preparation was carried out at room temperature. IMEs were cleaned using Piranha solution (96% H_2SO_4/30% H_2O_2; 3:1 (Caution: this solution reacts violently with organic compounds and should be handled with extreme care)), followed by brief sonication in deionized water and rinsing with water. Ethanol was used to further clean the IMEs before drying with nitrogen. ADT or DCA function as a mediator or cross-linking agent. The mediator to nanoparticle ratio was controlled, typically about (100−2000):1 depending on the chain length. The precleaned substrates or devices were immersed vertically into the assembly solution to ensure that the film formed was free of powder deposition. At a controlled immersion time, the film-deposited substrates were immersed and immediately rinsed thoroughly with hexane and dried under nitrogen before the characterization. The chain length for the thin films is denoted according to the number of $-CH_2-$ units (n) in ADT, which include $n = 3$, 5, 8, 9, and 10, or in DCA, which include $n = 10$, 12, 13, 14, 16, and 18. Figure 1 shows photos for both ADT−Au and DCA−AuAg thin films formed on IME devices. The films were uniform and the thickness could be controlled. In comparison with films prepared from the spraying and casting methods,[2,8−11] by which the interparticle interaction relies only on interdigitation of alkyl chains (i.e., VW interaction), there are a number of advantages for using the films assembled by bifunctional linkers in which the interparticle interactions involve both covalent Au−dithiolate−Au or Ag−dicarboxylate−Ag linkages and interdigitation of alkyl chains. The advantages include better morphological uniformity, increased structural stability, and better reproducibility, especially when organic vapors are adsorbed into the film.

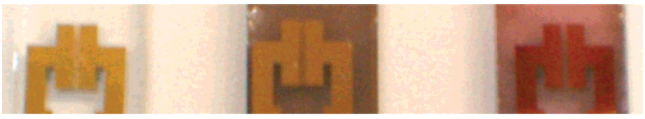

Figure 1. Photos showing IME (a), ADT−Au thin film on IME ($n = 10$) (b), and DCA−AuAg thin film on IME ($n = 16$) (c).

Devices and Measurements. Sensor response measurements were performed using an array of IME devices, with 100 pairs of gold electrodes of 200 μm length, 10 μm width, and 5 μm spacing on a 1-mm thick glass substrate (thickness of the Au electrodes: 100 nm). The IMEs were fabricated by a standard microfabrication technique using the Cornell NanoScale Science and Technology Facility (CNF). Details for the microfrabrication of the IMEs were reported previously.[13] The thickness of the coating was below or close to the finger thickness. A computer-interfaced multichannel multimeter (Keithley, Model 2700) was used to measure the lateral resistance of the nanostructured coating on the IME. All experiments were performed at room temperature, 22 ± 1 °C. N_2 gas (99.99%, Airgas) was used as a reference gas and as diluent to change vapor concentration by controlling the mixing ratio. The gas flow was controlled by a calibrated Aalborg mass-flow controller (AFC-2600). The flow rates of the vapor stream were varied between 3 and 99 mL/min, with N_2 added to a total of 100 mL/min. The vapor generating system consisted of a stainless steel multichannel module linked to different vapor bubblers (Teflon material). The modular platform components permitted different vapor flows with minimum dead-volume and virtually no cross-contamination. The vapor concentration was controlled by a flow system bubbling dry N_2 gas through a selected vapor solvent.

The IME devices were housed in a Teflon chamber with tubing connections to vapor and N_2 sources; the electrode leads were connected

(27) (a) Leibowitz, F. L.; Zheng, W. X.; Maye, M. M.; Zhong, C. J. *Anal. Chem.* **1999**, *71*, 5076. (b) Han, L.; Maye, M. M.; Leibowitz, F. L.; Ly, N. K.; Zhong, C. J. *J. Mater. Chem.* **2001**, *11*, 1258. (c) Kariuki, N. N.; Luo, J.; Hassan, S. A.; Lim, I.-Im S.; Wang, L. Y; Zhong, C. J. *Chem. Mater.* **2006**, *18*, 123.
(28) (a) Zellers, E. T.; Pan, T. S.; Patrash, S. J.; Han, M.; Batterman, S. A. *Sens. Actuators B* **1993**, *12*, 123. (b) Bakken, G. A.; Kauffman, G. W.; Jurs, P. C.; Albert, K. J.; Stitzel, S. S. *Sens. Actuators B* **2001**, *79*, 1. (c) Gardner, J. W. *Sens. Actuators B* **1991**, *4*, 109. (d) Corcoran, P.; Lowery, P.; Anglesea, J. *Sens. Actuators B* **1998**, *48*, 448.
(29) Polikar, R.; Shinar, R.; Udpa, L.; Porter, M. D. *Sens. Actuators B* **2001**, *80*, 243.
(30) (a) Brust, M.; Walker, M.; Bethell, D.; Schiffrin, D. J.; Whyman, R. *J. Chem. Soc., Chem. Commun.* **1994**, *7*, 801. (b) Hostetler, M. J.; Wingate, J. E.; Zhong, C. J.; Harris, J. E.; Vachet, R. W.; Clark, M. R.; Londono, J. D.; Green, S. J.; Stokes, J. J.; Wignall, G. D.; Glish, G. L.; Porter, M. D.; Evans, N. D.; Murray, R. W. *Langmuir.* **1998**, *14*, 17. (c) Maye, M. M.; Zheng, W. X.; Leibowitz, F. L.; Ly, N. K.; Zhong, C. J. *Langmuir.* **2000**, *16*, 490−497.
(31) Kariuki, N. N.; Luo, J.; Maye, M. M.; Hassan, A.; Menard, T.; Naslund, H. R.; Lin, Y.; Wang, C.; Engelhard, M. H.; Zhong, C. J. *Langmuir.* **2004**, *20*, 11240.

to the multimeter. Nitrogen was used as a carrier gas. Different concentrations of vapors were generated using an impinger system. At the beginning of the experiment, the test chamber was purged with pure nitrogen for 1 h to ensure the absence of air and also to establish the baseline. The test chamber was purged with N_2 and the analyte vapor alternately. A series of vapor concentrations was tested. The vapor concentration in the unit of ppm moles per liter was calculated from the partial vapor pressure and the mixing ratio of vapor and N_2 flows. Details of the measurement protocols were described previously.[6,12,13] ΔR is the difference of the maximum and minimum values of the resistance in response to vapor exposure, and R_i is the initial resistance of the film.[4] The sensitivity data were based on the relative differential resistance change, $\Delta R/R_i$, versus vapor concentration, C (ppm). The concentration given in ppm (M) in this paper, which can be converted to ppm (V) (which was often used in the literature) by multiplying a factor of 24.5,[6,12,13] was for convenience in thermodynamic analysis.

Results and Discussion

1. Response Characteristics of ADT−Au Array. The measured resistance (R_Ω) is related to the lateral conductivity (σ) of the film by the relationship of $\sigma = (1/R_\Omega)(w/dL)$, where w is the gap width of the array electrodes, L is the length of the electrodes, and d is the film thickness.[6] The thickness of the film with a specific chain length was controlled by assembly time. The initial resistance (R_Ω) of the film was found to decrease exponetionally with assembly time for ADT−Au films, suggesting that only the initial increase of film thickness has an effect on the resistance (see Supporting Information).

Figure 2A shows a representative set of the initial resistance measured for thin film assmblies of DT-capped gold nanoparticles mediated by ADTs of different chain lengths. The resistance clearly displays an exponetntial rise vs the chain length. This relationship is quite consistent with the overall electronic conduction mechanism in which the electron hopping and/or electron tunneling are dependent on the interparticle distance. The electrical conductivity depends on the core radius (r), interparticle distance (d), permittivity constant (ϵ_0), and dielectric constant of interparticle medium (ϵ) by a thermally activated conduction path[26,32]

$$\sigma = \sigma_0 \exp\left(-\frac{E_a}{RT}\right) \quad (1)$$

where the activation energy (E_a) is

$$E_a = 0.5e^2\frac{r^{-1} - (r+d)^{-1}}{4\pi\epsilon\epsilon_0} \quad (2)$$

Each addition of $-CH_2-$ in the alkyl chain leads to an increase of 0.13 nm spacing. The interparticle distance (d) is related to chain length (n) by the relationship $d = 1.5 + 0.13n$ (nm). The remarkable fitting of the resistance as a function of interparticle distance by eqs 1 and 2 ($R_\Omega \propto 1/\sigma$), as shown in Figure 2A, demonstrates that the electrical conduction in the thin film assembly follows a thermally activated conduction path. This conduction path is also consistent with measurement of the temperature dependence of the conductivity for thin films with different alkyl chain lengths (Figure 2B). A further comparison of the activation energy for the thin films derived

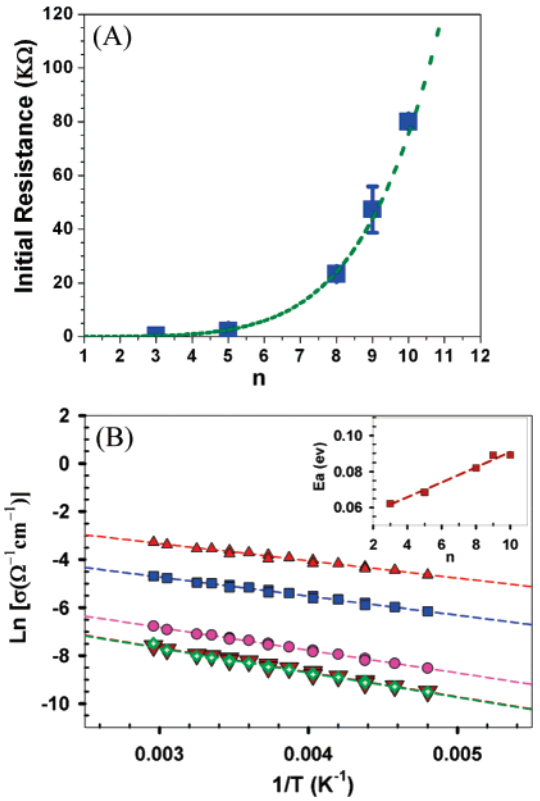

Figure 2. (A) Initial resistance of thin film assemblies of gold nanoparticles mediated by ADT ($HS-(CH_2)_n-SH$) of different chain lengths, i.e., n (number of methylene units in alkyl chain). Fitting result using eqs 1 and 2 ($R_i = 5130.9 \exp[-31.2/(1.5 + 0.13n)]$). (B) Dependence of conductivity on temperature for thin film assemblies of gold nanoparticles linked by ADTs of different chain lengths: $n = 3$ (red, triangle up), 5 (blue, square), 8 (pink, circle), 9 (dark red, diamond dotted), 10 (green, triangle down). Insert: E_a vs n (squares: experimental data; dashed line: linear regression, $E_a = 0.0040n + 0.0489$).

from different chain lengths shows an approximate linear relationship (Figure 2B insert), yielding 0.004 eV per methylene unit. The observation of the linear relationship is in agreement with those for layer-by-layer stepwise assemblies of gold nanoparticles reported by Brust and co-workers.[32]

While a detailed assessment of the chain length dependence of the electrical conductivity will be reported separately, the fitting results demonstrate that the electrical properties can be fine-tuned by the interparticle distance through the mediator linkers, which constitute the basis for the design of our sensor array films. The adsorbed VOCs studied in this work were all hydrophobic hydrocarbons which have a dielectric constant similar to that for the interparticle alkyl chains ($\epsilon \sim 2$). Since the nanoparticles are linked by dithiolates, thermal motion of the particles should be negligent. Thus, the main contribution to the resistivity response comes from the change in interparticle distance, which is in contrast to other vapors such as methanol and water which produce a significant contribution from dielectric properties to the resistivity change as reported previously.[6] Furthermore, the interparticle alkyl structures could be partially disordered because the interaction involves a combination of two forces: the dithiolate linkage and the capping alkyl chain interdigitation, which was termed as mediator−template interaction.[34] There is thus a compromised

(32) (a) Bethell, D.; Brust, M.; Schiffrin, D. J.; Kiely, C. J. *J. Electroanal. Chem.* **1996**, *409*, 137. (b) Brust, M.; Bethell, D.; Kiely, C. J.; Schiffrin, D. J. *Langmuir* **1998**, *14*, 5425.

(33) Nuzzo, R. G.; Dubois, L. H.; Allara, D. L. *J. Am. Chem. Soc.* **1990**, *112*, 558.

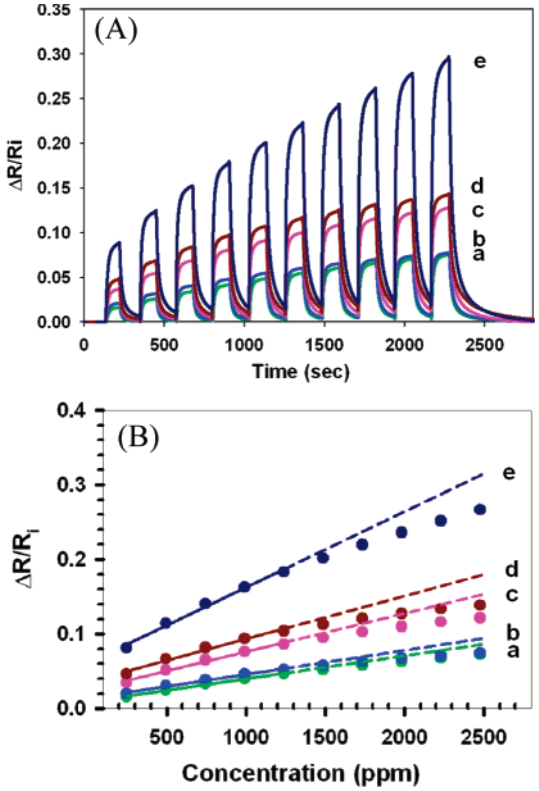

Figure 3. Sensor response profile (A) and sensitivity (B) to Hx vapor for ADT−Au films (see Supporting Information for response data of the same films to Bz and Tl vapors). ADT−Au films: $n = 3$ (a, green), 5 (b, light blue), 8 (c, pink), 9 (d, dark red), 10 (e, dark blue) linked thin films of Au nanoparticles (the vapor concentration unit: ppm(M) (ppm(M) × 24.5 = ppm(V))[6,12,13]).

balance of these two forces in order to maximize the overall interaction. The measured activation energy reflects the effect from an average of these two forces. For sensor responses described below, any slight imbalance of these two forces induced by vapor sorption could cause a change in interparticle distance and thus the film resistivity.

An example array consisting of ADT−Au thin films with $n = 3$, 5, 8, 9, and 10 was examined. Figure 3 shows a typical set of sensor response profiles for this sensor array, along with the dependence of the sensor response on vapor concentration. The response profile features an increase in $\Delta R/R_i$ upon exposure to the vapor which returns to baseline upon purge with nitrogen. The response is rapid and reversible. In most cases, the responses increased linearly with vapor concentration when the concentration was not too high. The slope serves as a measure of the response sensitivity (S). Deviation from the linear relationship occurs when the vapor concentration is high, which is due to the existence of a saturation effect or the complication of both bulk and surface adsorption phenomena.[6] For the convenience of an overall assessment, we used the linear approximation for assessing the sorption data. The fact that the linear plots in Figure 3 do not go through the origin is due to a combination of the background signal and the difference of linearity between the responses at low and high concentrations. Similar phenomena have been observed for other types of sensors for VOCs,[4,5] as discussed previously.[6]

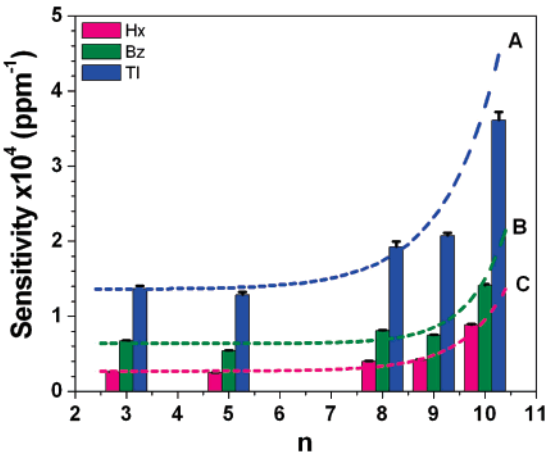

Figure 4. Response sensitivities (S) of a sensor array of ADT−Au thin films with different chain lengths to vapors of Tl (A, blue), Bz (B, green), and Hx (C, pink). Fitting results: S (S_0, a, b) = $S_0 + a \exp(bn)$; Hx: (2.71×10^{-5}, 5.44×10^{-10}, 1.16); Bz: (6.38×10^{-5}, 6.65×10^{-11}, 1.39); Tl: (1.36×10^{-4}, 2.08×10^{-8}, 0.93).

By comparing the vapor response sensitivities of the nanoparticle thin film assemblies derived from different chain lengths (Figure 4), a general trend of an exponential rising is evident for the response sensitivity vs chain length. This trend demonstrates the viability of fine-tuning the response sensitivity of the thin-film-coated chemiresistor sensors by interparticle distance in the nanostructure. This dependence is less significant for thin films derived from mediators with alkyl chains shorter than $n = 9$.

The issue of the possible effect of film thickness on the sensor response senstivity was addressed by examining the dependence of the sensitivity vs the relative thickness (see Supporting Information). The sensitivity was found to be dependent on the thickness only for very thin films with a relative thickness < 100. For relatively thicker films, the sensitivity is essentially independent of the film thickness. The fact that the films tested were all relatively thicker substantiated the comparison of the response sensitivity data in Figure 4.

2. Response Characteristics of DCA−AuAg Array. The sensing array consisting of DCA-mediated thin film assemblies of DT-capped AuAg nanoparticles allowed us to examine the effect of longer alkyl chain lengths on the sensor response sensitivity. An example array consisting of DCA−AuAg thin films with $n = 10$, 12, 13, 14, 16, and 18 was examined. These films differ from each other in terms of the chain length of the mediator molecule and, therefore, the interparticle spacing. The initial resistance values for the IME array of thin films were also measured. Similar to that for the array of ADT−Au thin films, the resistance of the thin films was found to decrease with assembly time, i.e., film thickness (see Supporting Information). The difference in the initial resistances reflects the difference in film thickness. The dependence of the resistance on the chain length of DCAs was found to display an exponetntial rise vs the chain length, similar to the case of the ADT−Au films.

The response profiles for a sensing array of six DCA−AuAg thin film materials on IME devices in response to VOCs were first examined. Figure 5 shows a representative set of response

(34) (a) Han, L.; Luo, J.; Kariuki, N. N.; Maye, M. M.; Jones, V. W.; Zhong, C. J. *Chem. Mater.* **2003**, *15*, 29. (b) Maye, M. M.; Luo, J.; Lim, I. S.; Han, L.; Kariuki, N. N.; Rabinovich, D.; Liu, T.; Zhong, C. J. *J. Am. Chem. Soc.* **2003**, *125*, 9906. (c) Lim, I. S.; Maye, M. M.; Luo, J.; Zhong, C. J. *J. Phys. Chem.* **2005**, *109*, 2578.

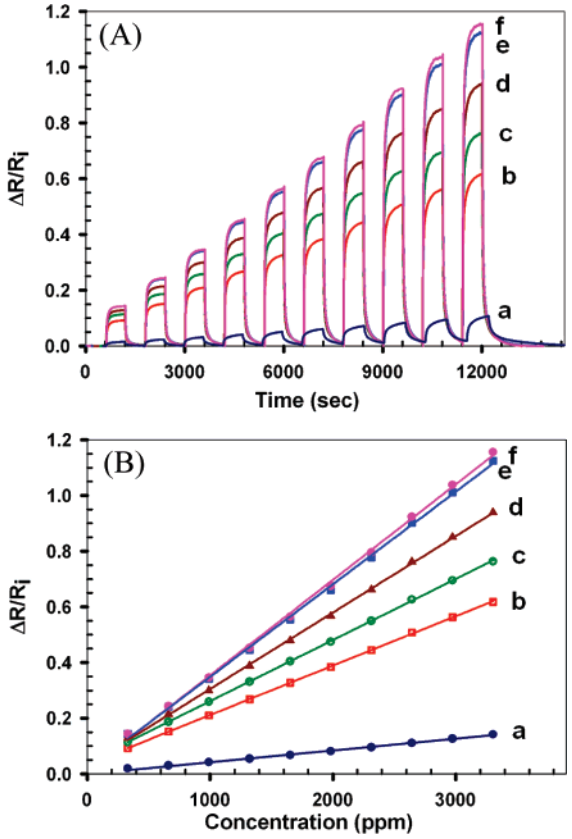

Figure 5. Sensor response profile (A) and sensitivity (B) to Hx vapor for DCA−AuAg films (see Supporting Information for the response data of the same films to Bz and Tl vapors). DCA−AuAg films: $n = 10$ (a, dark blue), 12 (b, red), 13 (c, green), 14 (d, brown), 16 (e, blue), and 18 (f, pink) linked thin films of AuAg nanoparticles.

characteristics for a six-sensor array. The response profiles for a selected set of vapor concentrations are displayed, and the corresponding response sensitivities are plotted against concentration. Again, the sensing array displays linear responses to concentrations of the vapors. While the response profiles of the same vapors at different films are similar, the response sensitivities vary dramatically, as evidenced by the differences in the slopes of the linear relationships. In contrast to those observed for ADT−Au films, little deviation from the linear relationship was observed, suggestive of the lack of a saturation effect or the complication of both bulk and surface adsorption phenomena for this type of thin films.

The dependence of the VOC response sensitivities on chain length (Figure 6) revealed an exponential rise to a maximum as a function of the chain length, demonstrating again the sensitivity of the sensor response to interparticle distance in the nanostructure. This trend reflects in part an increase of the interparticle nanoscale porosity with chain length and, in part, a decrease of the electrical conductivity of the thin film assembly with chain length. The chain length dependence of the electrical conductivity was in fact demonstrated in a previous report.[27,32] This finding is significant because it suggests the nanostructured sensing properties can be fine-tuned at the molecular level. Further insights into the sensor response and chain length correlation are gained by thermodynamic analysis of the sensor response characteristics and statistical analysis of the sensor array performance, as described next.

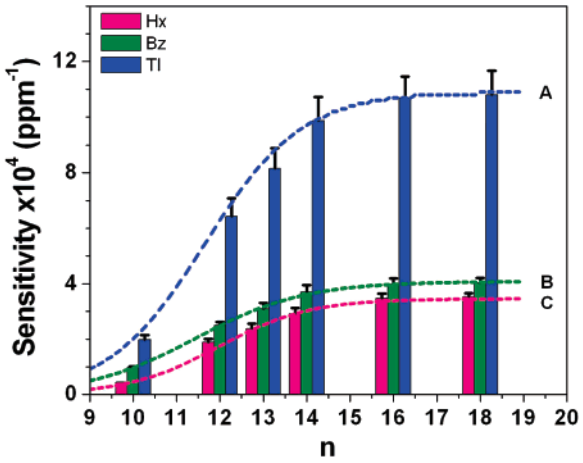

Figure 6. Response sensitivities of a sensor array of DCA−AuAg thin films with different chain lengths to vapors of Tl (A, blue), Bz (B, green), and Hx (C, pink) vapor. Fitting results: $S(a, b, c) = a/(1 + \exp(-(n - c)/b))$; Hx: $(3.46 \times 10^{-4}, 1.05, 11.97)$; Bz: $(4.08 \times 10^{-4}, 1.25, 11.45)$; Tl: $(1.09 \times 10^{-3}, 1.11, 11.65)$.

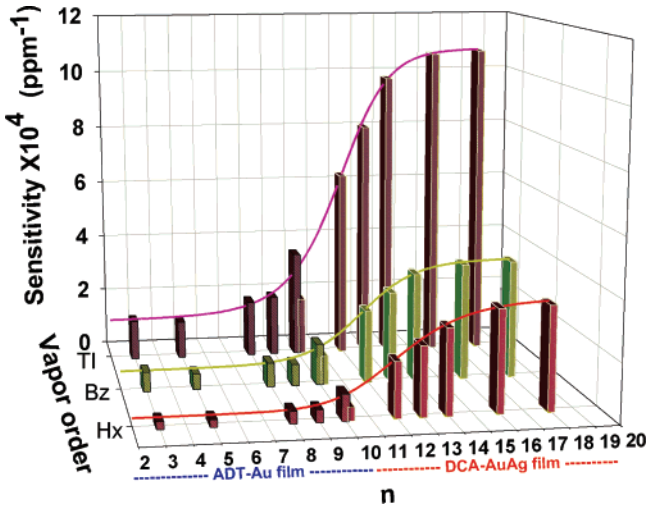

Figure 7. Response sensitivities of ADT−Au and DCA−AuAg thin films with different chain lengths to vapors of Tl, Bz, and Hx. Fitting results (Sigmoidal): $S(a, b, c, S_0) = S_0 + a/(1 + (n/c)^b)$; Hx: (3.38, −9.52, 12.22, 0.27); Bz: (3.47, −10.46, 11.84, 0.64); Tl: (9.58, −10.49, 11.92, 1.49).

3. Thermodynamic Assessment of Chain Length Dependence of Response Characteristics. Since the difference in particle sizes between Au and AuAg nanoparticles is rather small, they can be approximately considered as chemically inert nano building blocks of similar sizes, whereas the combination of the variable number of methylene units in the linking alkyl chain (ADT and DCA) and the fixed number of methylene units in the capping alkyl chain (DT) define the tunability in interparticle spacing. This approximation was supported by the observation of comparable conductivity values for the two types of thin films.[27] The chain length dependence of response characteristics obtained by combining the data for both ADT−Au and DCA−AuAg thin films with different chain lengths (Figure 7) is found to display a general trend characteristic of a sigmoidal feature. Clearly, the interparticle spatial properties must have played a dominant role in the sensor response characteristics.

The data revealed not only a clear dependence of the sensitivity on the alkyl chain length but also the occurrence of a dramatic change of the sensitivity in a region of the chain

Scheme 2. Illustrations of the Interparticle Structures Depending on the Relative Length Difference of the Interparticle Mediating/Linking Alkyl Chain (n in X−$(CH_2)_n$−X) and the Capping/Templating Alkyl (m in S−$(CH_2)_{m(m=9)}$−CH_3) Chains

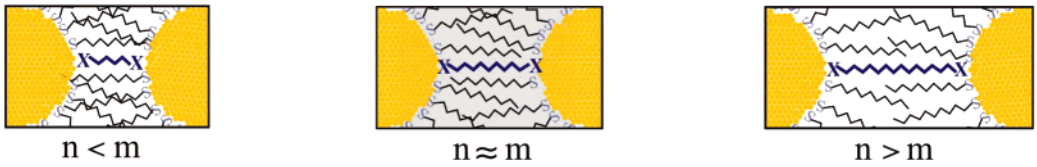

length for the alkyl mediator comparable with that of the capping alkyl chains, reflected by two important facts. First, the films with longer alkyl chains display a higher response sensitivity than those with shorter alkyl chains. This fact can be explained by the larger volume fraction of organic structures in the long-chain case which favors the sorption of the organic vapor into the film. The partition of vapor molecules in the film leads to an increased interparticle spacing, which changes the conductivity more significantly for the longer chain films than that for the shorter chain films. Second, the most significant change in the sigmoidal dependence of the sensitivity on chain length occurs in the range $n = 9-13$. This fact was further analyzed by considering the thermodynamic equilibrium for vapor sorption in the films of different chain lengths. Based on partition equilibrium constant (K_n), $K_n = C_n(\text{film})/C_v(\text{vapor})$, where C_n is the vapor concentration in the film with an alkyl chain length of n at the vapor-phase concentration, C_v ($C_v = \Delta R/(R_i \times S)$, the relative concentration ratio, which is related to the free energy of adsorption, $\Delta G_{ads} = -RT \ln K$, can be expressed as $C_n/C_{n'} = K_n/K_{n'} = \exp(-\Delta(\Delta G)/RT)$. By a rough estimate based on the difference of cohesive energies between two neighboring chain lengths (e.g., $n = 10$ and $n' = 9$), i.e., $\Delta(\Delta G) = \sim 0.8$ kcal /mol,[33] the $C_{n'=10}/C_{n=9}$ ratio would be ~4. The increase of 1 methylene unit would lead to an increase in the amount of vapor sorption into the film by a factor ~4, which is in fact quite consistent with the relative change of the thin film resistance in response to exposure of the vapor (see Figures 3 and 4). The fact that the significant change of response sensitivity occurs in the range $n = 9-13$, beyond which the dependence becomes less significant, is therefore believed to reflect the interparticle spatial and structural effects on the relative change of the electrical conductivity due to the relative length differences of the interparticle $-(CH_2)_n-$ structures defined by both mediating (or linking) and the capping (or templating) molecules (Scheme 2). The squeezed chain−chain interaction for the interparticle packing was discussed in our previous report.[34] Such a subtle difference constitutes an important thermodynamic factor for fine-tuning the vapor−nanostructure interactions. For $n = 9-13$, the linking molecular length falls in the vicinity of the capping DT, $m = 9$. As such, the vapor molecules enter a well-interdigitated mediating/capping alkyl structures. The perturbation of the interparticle distance is thus very sensitive to the mediator chain length. When $n < m$, the electrical conductivity of the film is relatively high and the organic volume fraction is relatively small so that the alkyl chains are not well interdigitated. In this case, the change in conductivity in response to the sorption of vapor molecules into the film is less sensitive to n in comparison with those for $n \approx m$. When $n > m$, the conductivity is relatively low and the organic volume fraction is relatively large. In this case, the interparticle alkyl chains cannot be well interdigitated. The change in conductivity in response to the sorption of vapor molecules into the film is thus less sensitive to n in comparison with those for $n \approx m$. It is apparent that there is a compromised balance between the interparticle chain−chain cohesive interdigitation and the chain−vapor interaction which determines the relative change of electrical conductivity of thin film in response to vapor sorption. In comparison with the use of thin films of unlinked particles as sensing materials which are often reported by others, the nanoparticles in our thin films are linked by dithiolates or dicarboxylates in which the thermal motion of the particles can be negligent. The major contribution to the change in electric conductivity in these thin films is thus from the vapor-induced change of interparticle distance.

Table 1. Results Based on Curve Fittings of the Data in Figure S5 (Supporting Information)

chain length (n)	F	k_f (s^{-1} M^{-1})	k_b (s^{-1})	K (M^{-1})	ΔG (kcal/mol)
5	0.111	50.0	0.069	721	3.88
8	0.167	68.8	0.080	857	3.98
9	0.188	125.0	0.134	930	4.03
12	0.838	13.1	0.051	258	3.28
14	1.518	11.5	0.057	200	3.13
16	1.251	15.7	0.051	317	3.40

The sorption equilibrium can also be analyzed by considering the kinetics in response to the sorption of vapor (e.g., hexane):

$$\mathrm{Hx_v} + \mathrm{Film} \underset{k_b}{\overset{k_f}{\rightleftharpoons}} \mathrm{Hx_{ad}/Film} \qquad (3)$$

where hexane in the vapor phase, Hx_v, adsorbs at a "binding site" in the film (Hx_{ad}/Film). k_f and k_b define the forward and backward rate constants, respectively. By assuming a Langmuir adsorption isotherm, which is reasonable for a process involving only hydrophobic interactions, the surface coverage (θ) ($\theta = \Gamma_t/\Gamma_0$, where Γ_t and Γ_0 represent coverage at time t and maximum coverage) at a given vapor concentration (C_v) can be derived as

$$\theta = a[1 - \exp(-bt)] \qquad (4)$$

where $a = C_v/(C_v + K^{-1})$, $K = k_f/k_b$, $b = k_f C_v + k_b$. On the basis of the response data characteristics, it is reasonable to relate the $\theta(t)$ to the change of the measured resistance, $\Delta R/R_i = F\theta(t)$, where F is a proportionality factor. By fitting the transient response data for different vapor concentrations by eq 4 (see Supporting Information), values of F and the rate constants (k_f and k_b) were determined for each film, which allow the equilibrium constant K and ΔG_{ads} to be estimated (Table 1).

The values of $-\Delta G_{ads}$ (4.0−3.4 kcal/mol) were found to fall in between those expected for the condensation energy of hydrocarbons (~6 kcal/mol)[35] and those reported for the cohesive energy of alkyl chains (i.e., 1.4−1.8 kcal/mol[33]). This

(35) Cogen, J. M.; Maier, W. F. *Langmuir* **1985**, *3*, 830.

Table 2. General Full Factorial Design for ADT−Au and DCA−AuAg Sensors

	(I) ADT–Au film array					(II) DCA–AuAg film array					
level	1	2	3	4	5	1	2	3	4	5	6
factor I: chain length	3	5	8	9	10	10	12	13	14	16	18
factor II: vapor	Hx	Bz	Tl			Hx	Bz	Tl			

Table 3. ANOVA Results for the Sensitivity of ADT−Au and DCA−AuAg Sensing Films

source of variation	degrees of freedom	sequential sum of squares	adjusted sum of squares	adjusted mean square	F_0[a]	*P*-value
			ADT−Au			
n	4	235.25	235.25	58.81	5.19	0.023
vapor	2	606.21	606.21	303.10	26.75	0
error	8	90.65	90.65	11.33		
total	14	932.11				
			DCA−AuAg			
n	5	6291.2	6291.2	1791.5	61.67	0.007
vapor	2	13215.8	13215.8	6607.9	32.81	0
error	10	2013.9	2013.9	201.4		
total	17	21521.0				

[a] F_0: value of F-test in ANOVA analysis.

result is consistent with the nature of the hydrophobic interaction of hexane vapor with the alkyl network in the nanoparticle thin film assembly. Interestingly, the values of K_n for shorter alkyl chains are found to be larger than those of $K_{n'}$ for longer alkyl chains. The ΔG_{ads} values display a subtle transition at $n = \sim 10$ from ~ -4.0 kcal/mol for the shorter chain films to ~ -3.4 kcal/mol for the longer chain films. This transition region coincides with the transition region of the response sensitivity (Figure 7), reflecting the important role played by the thermodynamic factor in the nanostructured sensing properties.

These findings have significant implications to the design of sensing nanostructures in terms of interparticle spatial properties. It is apparent that the combination of mediator $(-(CH_2)_n-)$ and capping $(-(CH_2)_m-)$ molecules in the nanostructured thin films at a given particle size determines the thermodynamic equilibrium for the vapor sorption. A further study of the effect of the variation of *m* in the capping molecule of $X-(CH_2)_mCH_3$ on the sensing properties is expected provide additional insights into the fine engineering of the interparticle mediating/templating interactions of the nanostructured sensing materials.

4. Statistical Assessment of the Sensor Array Performance. To further evaluate the response characteristics of the sensor arrays with the different interparticle spacing properties, Analysis of Variance (ANOVA) techniques were used to analyze the data in terms of sensitivity and selectivity. There are two factors, the interparticle spatial parameter and the vapor type, which are involved in a general full factorial experiment. As described in this subsection, the selectivity characteristics were evaluated by calculating the Euclidean distance among vapor response curves, and the thin films with different chain lengths were assessed with the Principal Component Analysis (PCA) method.

The general full factorial experiments for ADT−Au and DCA−AuAg sensor arrays were designed with the experiment parameters summarized in Table 2, in which each experiment has two factors: interparticle spatial parameter with five levels for ADT−Au and six levels for DCA−AuAg sensors, and vapor types with three levels for each type of sensor. The normalized

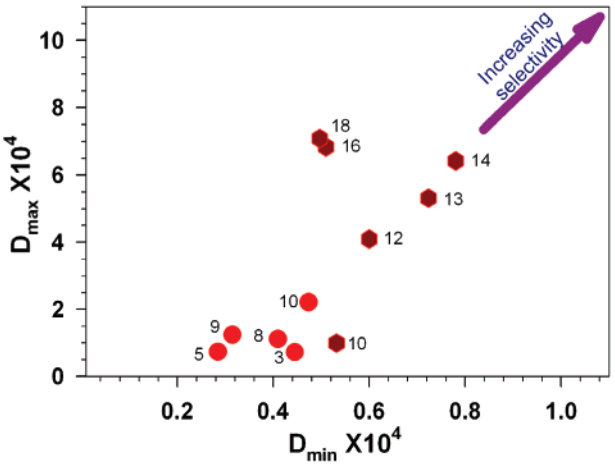

Figure 8. Scatter plot in D_{max} vs D_{min} plane for sensor arrays based on ADT−Au (n = 3, 5, 8, 9, 10) (circle) and DCA−AuAg (n = 10, 12, 13, 14, 16, 18) (hexagon) films.

Table 4. ANOVA Results for the D_{max} Measure of ADT−Au and DCA−AuAg Films

source of variation	sum of squares	degrees of freedom	mean square	F_0	*P*-value
		ADT−Au			
n	4	1177.540	294.385	565.680	0.000
error	31	16.133	0.520		
total	35	1193.673			
		DCA−AuAg			
n	5	4155.400	831.100	17.140	0.000
error	10	484.900	48.500		
total	15	4640.400			

Table 5. ANOVA Results for the D_{min} Measure ADT−Au and DCA−AuAg Films

source of variation	degrees of freedom	sum of squares	mean square	F_0	*P*-value
		ADT−Au			
n	4	5.236	1.309	7.880	0.035
error	4	0.665	0.166		
total	8	5.901			
		DCA−AuAg			
n	5	10.346	2.069	8.020	0.020
error	5	1.290	0.258		
total	10	11.636			

response sensitivities of the ADT−Au films (five different chain lengths) and the DCA−AuAg films (six different chain lengths) to the three different vapors (hexane, benzene, and toluene) were used as the performance measures for the evaluation. The average of the three duplicate measurements on the responses for each of ADT−Au and DCA−AuAg films serves as the experimental response.

The experimental results were analyzed with the ANOVA method. The factors (or parameters) with a *P*-value smaller than a significant level α were considered as significant factors. Table 3 summarizes the ANOVA results of sensitivity for the two different films respectively. The *P*-values for interparticle spatial parameter and vapor type were all found to be smaller than the significant level ($\alpha = 0.05$). It is therefore concluded that both the interparticle spatial parameter and the vapor type have a significant influence on the sensitivity.

The above experimental data were further analyzed using our selectivity evaluation technique.[12] The selectivity characteristic

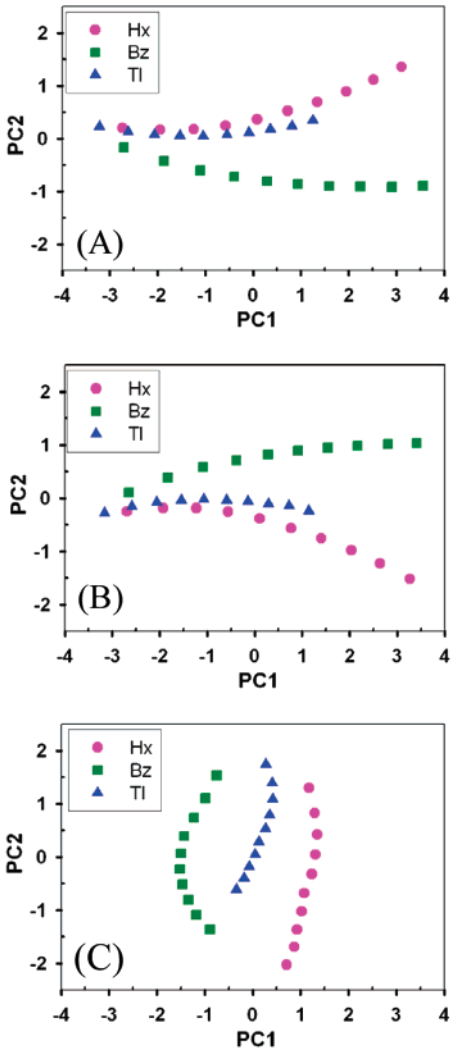

Figure 9. PCA score plots in the PC1−PC2 plane for three sensor arrays: (A) ADT−Au ($n = 3$ and 5) and DCA−AuAg ($n = 12$ and 13); (B) ADT−Au ($n = 3$ and 5) and DCA−AuAg ($n = 16$ and 18). (C) ADT−Au ($n = 9$ and 10) and DCA−AuAg ($n = 16$ and 18)). Vapor Tl (triangle, blue), Bz (square, green), and Hx (circle, pink).

of a thin film is measured with the Euclidean distances among the response curves for different vapors. The minimum distance (D_{min}) describes how well the two closest vapors response curves can be distinguished by a film, whereas the maximum separation distance (D_{max}) characterizes the film's highest separation capability. The selectivity characteristics, D_{min} and D_{max}, are summarized in Figure 8. A larger value for the measures means that the film has a better capability to distinguish different vapors. A compromised balance between D_{min} and D_{max} seems to suggest that an array consisting of thin films with $n = 14$, 13, 12, 18, and 16 is desired.

To understand the effect of an interparticle spatial parameter on the film's selectivity characteristics, the results of D_{max} and D_{min} were analyzed with the ANOVA method. Tables 4 and 5 summarize the ANOVA results of D_{max} and D_{min} for the two different types of films. The finding that the *P*-values are all smaller than the significant level (0.05) for both D_{max} and D_{min} indicates that the chain length significantly influences the separation capability. The results suggest that the separation capability of the thin film array could be potentially enhanced by specifying the chain length for both ADT−Au and DCA−AuAg sensor arrays.

PCA analysis was used to visualize the capability of a sensor array in distinguishing different vapors, which allows the reduction of variable dimensions (feature extraction) and classification, and thus provide information for evaluating the performance of the sensor array with films of different chain lengths. To establish the relation between the classification capability of the sensor array and the interparticle spatial parameter of a thin film, sensor arrays with different combinations of the thin films with variant chain length for different vapors have been tested. The results showed that the classification capability of each array is highly dependent on the specific combination. For example, consider the sensor arrays with the following combinations: Array A consisting of ADT−Au and DCA−AuAg films with shorter chain lengths (ADT−Au ($n =$ 3 and 5) and DCA−AuAg ($n = 12$ and 13)); Array B consisting of ADT−Au films with shorter chain lengths and DCA−AuAg films with longer chain lengths (ADT−Au ($n = 3$ and 5) and DCA−AuAg ($n = 16$ and 18)); and Array C consisting of ADT−Au and DCA−AuAg films with longer chain lengths (ADT−Au ($n = 9$ and 10) and DCA−AuAg ($n = 16$ and 18)). The response data of these arrays to hexane, benzene, and toluene were analyzed. Figure 9 shows the PCA score plots in the PC_1−PC_2 plane for each of the three vapors with the normalized responses at 10 different concentration levels. The response patterns can be well separated with array C. For arrays A and B, while the response pattern for Bz is well separated from those for Hx and Tl, the latter two are overlapped at a lower concentration region. An implication is that the interparticle spatial parameter affects the classification capability. By appropriately selecting the combination of interparticle spatial parameters for the thin film array system, the classification capability can be significantly enhanced. Our ongoing work involves a more comprehensive analysis of the sensor array data, especially for vapor mixtures. In the case of vapor mixtures, the sensor array alone is not capable of recognizing the component. However, the array achieves recognition when it is coupled with a pattern recognition neural network,[12] the results of which will be reported in the near future.

Conclusions

In conclusion, the viability of a sensing array consisting of molecularly mediated thin film assemblies of metal nanoparticles with interparticle spatial properties defined by alkyl chains of different lengths has been demonstrated for the first time. The correlation between the VOC-response sensitivity and the interparticle spacing properties revealed not only a clear dependence of the sensitivity on the alkyl chain length but also the occurrence of a dramatic change of the sensitivity in a region of the chain length for the alkyl mediator comparable with that of the capping alkyl chains. In other words, the VOC−nanostructure van der Waals interaction induced perturbation to the conductivity depends on the relative alkyl chain length of the mediating $-(CH_2)_n-$ vs the capping (or templating) $-(CH_2)_m-$ structures. This finding is believed to reflect a compromised balance between the interparticle chain−chain cohesive interdigitation and the nanostructure−vapor interaction which determines the relative change of the electrical conductivity of the interparticle-linked thin film in response to vapor sorption. The increase of the response sensitivity and separation

capabilities with the interparticle spacing were also supported by statistical techniques such as analysis of variance and principal component analysis of the sensor array data in terms of sensitivity and selectivity. An important implication of the findings is the significance of the interparticle fine-tuning capability of the interparticle-linked thin film materials for the design of effective chemical sensor arrays.

Acknowledgment. Financial support of this work in part from National Science Foundation (CHE 0349040) and from the U.S. Department of Energy (NNSA) is gratefully acknowledged. The use of Cornell NanoScale Science & Technology Facility for device fabrication is also acknowledged.

Supporting Information Available: Additional thin film resistance and response data (Figures S1−S5). This material is available free of charge via the Internet at http://pubs.acs.org.

JA0673074